A Target-Free Automatic Self-Calibration Approach for Multibeam Laser Scanners

Zheng Gong, Chenglu Wen, *Member, IEEE,* Cheng Wang, *Senior Member, IEEE*, and Jonathan Li, *Senior Member, IEEE*

***Abstract*— In this paper, a target-free automatic self-calibration approach for multibeam laser scanners is proposed. The proposed approach uses the isomorphism constraint among the laser scanner data to optimize the calibration parameters, uses the ambiguity judgment algorithm to solve the mismatch problem, and finally achieves the purpose of automatic calibration. The experimental results show that the accuracy of our algorithm is higher than that of the target-based calibration approach. The calibration process is automatic and fast.**

***Index Terms*— Multibeam laser scanner, self-calibration, sensor, simultaneous localization and mapping, target free.**

I. Introduction

IN THE application of laser-based simultaneous localization and mapping and 3-D reconstruction [1], to further improve the mapping process, multisensor data fusion brings more robustness and higher precision to the algorithm and captures the 3-D environment in detail. Due to the limited view of a single-laser scanner sensor, multiple-laser scanner sensors are usually cross-mounted to more completely acquire 3-D data. In the multisensor system, sensors have their own local coordinates. To unify the coordinate system, the 3-D coordinate transformation relation between the laser scanners must be accurately calibrated.

Previously, a common approach to deal with the multisensor calibration is to achieve a common view of the sensors by introducing special calibration targets [2]. As a classical tool for laser scanner calibration, a pattern plane plays a significant role in extrinsic calibration of laser scanner. Atanacio *et al.* [3] and Muhammad and Lacroix [4] proposed the feature-constraint-based methods for multibeam laser scanner self-calibration. He *et al.* [5] used the multitype geometric feature (corner points, lines, and planes)-based algorithm to handle the pairwise light detection and ranging (LiDAR) calibration. These methods improve the accuracy of the calibration to a certain extent, but require special design targets with specific geometric features. In multibeam laser scanner calibration, to determine the corresponding target points or corner features in the common view of the sensor from the sparse point cloud is very difficult. An automatic intrinsic calibration approach for multibeam laser scanner is suggested by energy function but cannot handle extrinsic calibration [12].

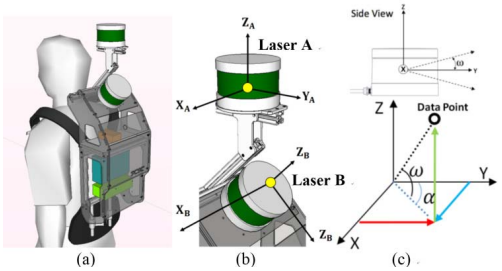

Fig. 1. (a) Our backpack 3-D scanning system. (b) Laser scanner A and laser scanner B's coordinates. (c) Coordinate of laser scanner.

In this paper, a target-free automatic self-calibration approach is proposed for multibeam laser sensors. The approach uses one LiDAR mapping in the first step, and then uses the isomorphism constraint among the data to optimize the calibration parameters with no target required. During calibration, generally mismatch in target registration may introduced, which brings errors into the statistical model. To eliminate the mismatch and achieve accurate automatic calibration, a mismatch elimination rule based on the statistical model is also developed. In comparison of target-based approach, our approach eliminates the need of external target, and thus fully automatic. Since the approach does not need the manually fitting to find the corresponding target point in sparse point cloud frame data, it also avoided the fitting error and achieves efficient and accurate self-calibration.

II. Data Acquisition and Coordinate System

A. Data Acquisition

Our calibration experiments were performed on a backpack 3-D scanning system [Fig. 1(a)]. The system uses two 16-line 3-D laser scanners (Velodyne VLP-16) [6], each composed of sixteen laser-detector pairs individually aimed in 2° increments over the 30° (−15° to +15°) field of view of the laser scanner [Fig. 1(b)]. The point cloud P (x, y, z) in the scanner's own coordinate system is identical to those calculated for VLP-16, as given in (1) and shown in Fig. 1(c).

B. Multisensor Coordinate System

Laser scanner A (Laser A) is placed horizontally and laser scanner B (Laser B) is mounted at 45 below it [Fig. 1(b)]. The point cloud data in the Cartesian coordinate system (X, Y, Z) are calculated for 3-D laser scanners in (1). Our goal is to determine a transform T_{cali} that places $P_{\text{Laser}A}$ and $P_{\text{Laser}B}$ in the same coordinate and merge them in P_{global} (2)

$$P = \begin{bmatrix} X \\ Y \\ Z \end{bmatrix} = \begin{bmatrix} R*\cos(\omega)*\sin(\alpha) \\ R*\cos(\omega)*\cos(\alpha) \\ R*\sin(\alpha) \end{bmatrix} \tag{1}$$

$$P_{\text{global}} = P_{\text{Laser}A} + T_{\text{cali}} * P_{\text{Laser}B}. \tag{2}$$

Manuscript received July 25, 2017; revised September 20, 2017; accepted September 22, 2017. This work was supported in part by the National Science Foundation of China under Grant 61771413 and Grant 4141379 and in part by the Fundamental Research Funds for the Central Universities under Grant 20720170047. The Associate Editor coordinating the review process was Dr. George Xiao. *(Corresponding author: Chenglu Wen.)*

Z. Gong, C. Wen, and C. Wang are with the Fujian Key Laboratory of Sensing and Computing for Smart City, School of Information Science and Engineering, Xiamen University, Xiamen 361005, China, and also with the Fujian Collaborative Innovation Center for Big Data Applications in Governments, Fuzhou 350003, China (e-mail: 770369550@qq.com; clwen@xmu.edu.cn; cwang@xmu.edu.cn).

J. Li is with the Fujian Key Laboratory of Sensing and Computing for Smart City, School of Information Science and Engineering, Xiamen University, Xiamen 361005, China, with the Fujian Collaborative Innovation Center for Big Data Applications in Governments, Fuzhou 350003, China, and also with the GeoSTARS Laboratory, Department of Geography and Environmental Management, University of Waterloo, Waterloo, ON N2L 3G1, Canada (e-mail: junli@xmu.edu.cn).

Color versions of one or more of the figures in this paper are available online at http://ieeexplore.ieee.org.

Digital Object Identifier 10.1109/TIM.2017.2757148

III. Target-Based Manual Calibration

For comparison, a sensor calibration experiment with feature-constraint target-based manual calibration was first conducted [4], and then, the proposed target-free automatic calibration experiment was conducted. In the target-based manual calibration experiment, two white square targets with a square hole were used and placed in the sensor's common view area (Fig. 2).

The detailed registration process of the feature-constraint target-based calibration approach is the following. First, several targets were placed in the scanning scene. Second, the target feature points (corner points, lines, and planes) were manually labeled and matched in the common view point cloud. Third, the target coordinates were transformed with coarse registration by the manually selected points. Finally, the point cloud registration algorithm (normal distribution transform [10]) was used for fine registration.

IV. Target-Free Automatic Self-Calibration Approach

A. Automatic Self-Calibration Algorithm

Instead of using the target-based approach, the sensors coordinate transformation in a large quantity of data is calculated in our method; that is, the calibration matrix is recursively computed in the continuous construction of the submap and its isomorphism constraint.

Based on the generalized-ICP algorithm [7] and LiDAR odometry and mapping (LOAM) [8] method, a precise local submap, M was built. Assuming T_A^n is laser scanner A's trajectory at time $(0-n)$ in the mapping algorithm, P_B^n is the laser scanner B's point cloud at time n. T_{guess} is the initial value of the coordinate transformation relation between the two sensors. T_{guess} is estimated by a coarse manual measurement. Among them, T_A^n and P_B^n are synchronized, with one-to-one correspondence. The output of the approach is to determine the exact calibration matrix T_{cali}.

Using the multilaser scanner system, the following data are obtained:

$$\begin{aligned}&\text{Given } \left(M, T_A^n, P_B^n, T_{\text{guess}}\right)(n=0\sim t)\\&\text{And } T_A^n \sim P_B^n(\text{synchronization})\\&\text{Find } T_{\text{cali}}.\end{aligned}$$

With the isomorphism and rigid coordinate constraints, the mathematical model for automatic calibration is introduced by

$$P_A^n = NN\left(M, T_A^n, P_B^n, T_{\text{guess}}\right) \tag{3}$$

$$T_{\text{cali}} = \text{argmin}_{T_{\text{cali}}} \sum_n \left\| P_B^n * T_{\text{cali}} - P_A^n \right\|^2. \tag{4}$$

In (3), NN is the nearest neighbor point search algorithm in fast library for approximate nearest neighbors [9]. Based on the assumption that data and trajectories are synchronized, laser scanner B's point cloud P_B^n is transformed to its location at time n in the subusing T_A^n and T_{guess}. Then, the nearest neighbor search algorithm is applied to find the nearest neighbor point P_A^n on the sub-map. Finally, the environmental consistency constraint is introduced to deduce (4) to obtain T_{cali}^n.

For each set of corresponding point clouds, the ICP algorithm is used to obtain the minimum value with the initial transform T_{guess}

$$T_{\text{cali}}^1 = \text{ICP}\left(P_B^1, P_A^1, T_{\text{guess}}\right), \quad T_{\text{guess}} = T_{\text{cali}}^1 \tag{5}$$

$$T_{\text{cali}}^2 = \text{ICP}\left(P_B^2, P_A^2, T_{\text{guess}}\right), \quad T_{\text{guess}} = T_{\text{cali}}^2 \tag{6}$$

$$\cdots$$

$$T_{\text{cali}}^n = \text{ICP}\left(P_B^n, P_A^n, T_{\text{guess}}\right), \quad \text{Output}: T_{\text{cali}}^n \tag{7}$$

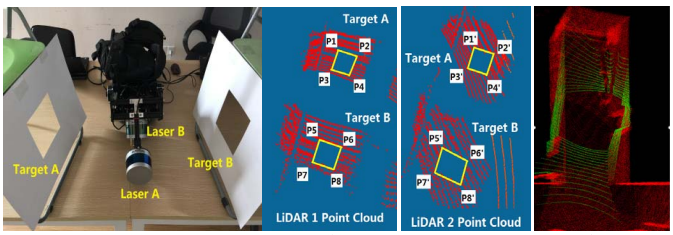

(a) (b) (c) (d)

Fig. 2. (a) Target-based calibration experimental scene. (b) Laser scanner A's point cloud. (c) Laser scanner B's point cloud. (d) Registering the point cloud (green point cloud) from laser scanner B to the local submap (red point cloud) from laser scanner A.

TABLE I
Calibration Errors of Two Methods

	Target-based Scene b1	Target-based Scene b2	Target-free Scene f1	Target-free Scene f2
x_error(mm)	*15.896*	*21.960*	*6.372*	*7.877*
y_error(mm)	*20.271*	*23.389*	*5.943*	*5.276*
z_error(mm)	*7.377*	*10.257*	*3.129*	*6.134*
Roll_error(deg)	*0.053*	*0.066*	*0.018*	*0.029*
Yaw_error(deg)	*0.060*	*0.013*	*0.022*	*0.019*
Pitch_error(deg)	*0.082*	*0.096*	*0.037*	*0.024*
RMS_T_error(mm)	*26.795*	*33.682*	*9.258*	*11.291*
RMS_R_error(mm)	*0.114*	*0.116*	*0.046*	*0.045*

B. Mismatch Problem and Its Solution

Ambiguity of the calibration environment (e.g., a long corridor) easily leads to the failure of the calibration algorithm. To deal with it, an ambiguity evaluation algorithm is proposed to filter the outliers and use multiple registration statistics to estimate the calibration matrix [(8) and (9)]. The random sample consensus (RANSAC) [11] method is used to remove the large error outliers. Then, the mean value is calculated to determine the final calibration matrix $T_{\text{cali}}^{\text{Final}}$

$$T_{\text{cali}}^{'} = \text{RANSAC}\left(T_{\text{cali}}^n\right) \tag{8}$$

$$T_{\text{cali}}^{\text{Final}} = \text{Mean}\left(T_{\text{cali}}^n\right). \tag{9}$$

V. Experimental Results

A. Target-Based Calibration Experiment

For target-based calibration approach in [4], the size of targets "A" and "B" at 400 × 400 mm^2 with hole size 200 × 200 mm^2 was designed and placed one meter away on the left and right sides of the system, respectively [Fig. 2(a)]. As shown in Fig. 2(b), the point cloud of the multibeam laser scanner is too sparse to locate the exact correspondence point in the common view area. Thus, the RANSAC fitting method was used to fit two squares (yellow squares) in the sparse point cloud, thereby locating the corresponding points on the square corner.

The target corner points $P_1 \sim P_8$ and $P_1^{'} \sim P_8^{'}$ [Fig. 2(b) and (c)] were used to analyze the error of the calibration matrix. After calibration, the average distance between the corresponding points of the target and the total least mean square error was calculated. Two groups of experimental errors (X, Y, Z, roll, yaw, pitch error and mean square error) are listed in Table I (scene b1 and scene b2).

B. Target-Free Calibration Experiment

Carrying our backpack system and walking along two corridor scenes, two sets of data (scene f1 and scene f2) were collected.

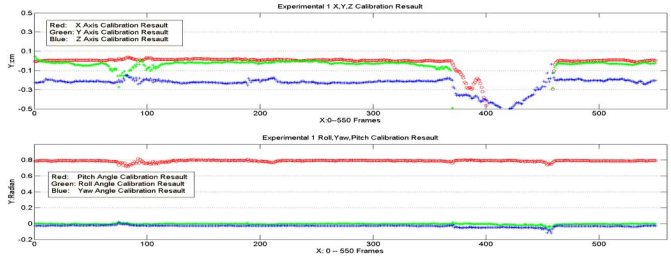

Fig. 3. Automatic self-calibration results.

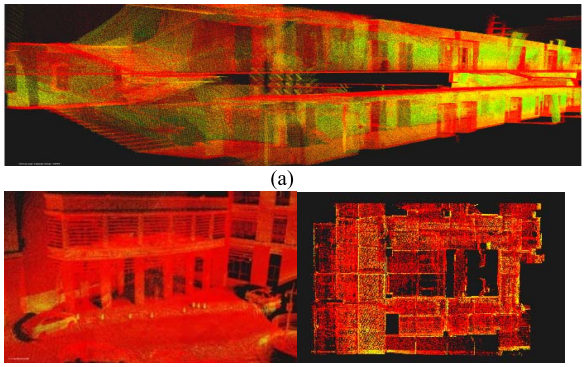

Fig. 4. Multilaser scanners mapping results for different scenes. (a) Two-floor corridor. (b) Outdoor. (c) Basement.

Each set of data includes 550-point cloud frames. The LOAM [8] method was used for short-term (550 frames) mapping of point cloud data collected by laser scanner A [red point cloud in Fig. 2(d)]. The data of laser scanner B [green point cloud in Fig. 2(d)] were rotated using initial value T_{guess} and synchronized transformed to the approximate nearest point location of the laser scanner A's local submap.

Fig. 3 shows the automatic calibration result from 0∼550 frames for scene f1 and scene f2. Our approach performs well between 100–360 frames, but becomes unstable after 360 frames. A generalized-ICP [7] was used in our approach to register the point cloud of laser scanner B to the local submap of laser scanner A. When the mapping system moving in an environment where obvious structural features are absent (e.g., long corridors), the generalized-ICP becomes unstable, causing mismatch and large errors. The ambiguity judgment algorithm was performed in this situation to remove outliers and achieve stable calibration results.

Target corner points were used to analyze the error of the calibration matrix. The average distances between the corresponding points of the target and the total least mean square error were calculated. Two groups of experimental errors (X, Y, Z, roll, yaw, pitch error, and mean square error) are listed in Table I.

In Table I, rms_T_ error is the x, y, z mean square root error, and rms_R_ error is the roll, yaw, and pitch root mean square error. Results indicate that both in rotation and drift calibration, our approach achieves better accuracy and robustness than the target-based calibration approach.

Our calibration approach can work in both indoor and outdoor scenes that have rich structural features (lines or corners). Fig. 4 displays the final multilaser scanner mapping results using the transformation matrix achieved by the proposed approach. The testing scene is a 30-m long, 2-m wide two-floor corridor [Fig. 4(a)]. Orange and yellow point clouds were acquired by laser scanner A and laser scanner B, respectively. Our calibration approach was also tested on outdoor [Fig. 4(b)] and basement scene [Fig. 4(c)]. The results indicate the data from the two calibrated sensors are well fused.

VI. Conclusion

This paper proposes a target-free automatic self-calibration approach for multibeam laser scanners using the isomorphism constraint and ambiguity judgment algorithm. The proposed calibration process is rapid and fully automatic. Experimental results show that our algorithm outperforms that of target-based calibration approach in precision.

References

[1] Y. Zhuang, N. Jiang, H. Hu, and F. Yan, "3-D-laser-based scene measurement and place recognition for mobile robots in dynamic indoor environments," *IEEE Trans. Instrum. Meas.*, vol. 62, no. 2, pp. 438–450, Feb. 2013.

[2] Y. Zhuang, F. Yan, and H. Hu, "Automatic extrinsic self-calibration for fusing data from monocular vision and 3-D laser scanner," *IEEE Trans. Instrum. Meas.*, vol. 63, no. 7, pp. 1874–1876, Jul. 2014.

[3] G. Atanacio-Jiménez *et al.*, "LiDAR Velodyne HDL-64E calibration using pattern planes," *Int. J. Adv. Robot. Syst.*, vol. 8, no. 5, pp. 70–82, 2011.

[4] N. Muhammad and S. Lacroix, "Calibration of a rotating multi-beam LiDAR," in *Proc. IEEE Int. Conf. Intell. Robots Syst.*, Oct. 2010, pp. 5648–5653.

[5] M. He, H. Zhao, F. Davoine, F. Cui, and H. Zha, "Pairwise LiDAR calibration using multi-type 3D geometric features in natural scene," in *Proc. Int. Conf. Intell. Robots Syst.*, Nov. 2013, pp. 1828–1835.

[6] *Velodyne PUCK (VLP-16) LiDAR*. Accessed: Jan. 20, 2016. [Online]. Available: http://velodynelidar.com/vlp-16.html

[7] A. Segal, D. Haehnel, and S. Thrun, "Generalized-ICP," *Robot., Sci. Syst.*, vol. 2, no. 4, p. 435, 2009.

[8] J. Zhang and S. Singh, "LOAM: LiDAR odometry and mapping in real-time," in *Proc. Robot., Sci. Syst. Conf. (RSS)*, Jul. 2014, pp. 1–9.

[9] *FLANN—Fast Library for Approximate Nearest Neighbors*. Accessed: Mar. 15, 2016. [Online]. Available: http://www.cs.ubc.ca/research/flann/

[10] M. Magnusson, "The three-dimensional normal-distributions transform: An efficient representation for registration, surface analysis, and loop detection," *Renew. Energy*, vol. 28, no. 4, pp. 655–663, 2009.

[11] M. A. Fischler and R. C. Bolles, "Random sample consensus: A paradigm for model fitting with applications to image analysis and automated cartography," *Commun. ACM*, vol. 24, no. 6, pp. 381–395, 1981.

[12] H. Nouira, J.-E. Deschaud, and F. Goulette, "Point cloud refinement with a target-free intrinsic calibration of a mobile multi-beam LiDAR system," in *Proc. Int. Soc. Photogramm. Remote Sens.*, vol. 3. 2016, pp. 359–366.